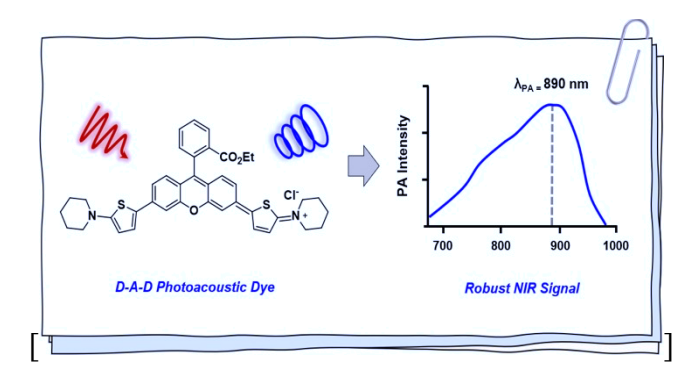
Thienylpiperidine donor NIR xanthene-based dye for photoacoustic imaging

Chathuranga S. L. Rathnamalala a ‡ Nicholas W. Pino, b ‡ Bailey S. Herring, a Mattea Hooper, a Steven R. Gwaltney, a Jefferson Chan b * and Colleen N. Scott a *

- a) Department of Chemistry, Mississippi State University, Mississippi State, MS 39762, United States
- b) Department of Chemistry, University of Illinois at Urbana-Champaign, Urbana, IL 61801, United States
- ‡) These authors contributed equally.

Supporting Information Placeholder



ABSTRACT: Few xanthene-based near-infrared (NIR) photoacoustic (PA) dyes with absorbance >800 nm exists. As accessibility to these dyes requires long and tedious synthetic steps, we designed a NIR dye (**XanthCR-880**) with thienylpiperidine donors and a xanthene acceptor that is accessible in 3-4 synthetic steps. The dye boasts strong PA signal at 880 nm with good biological compatibility and photostability, yields multiplexed imaging with an aza-BODIPY reference dye, and is detected at a depth of 4 cm.

Photoacoustic (PA) tomography is a state-of-the-art biomedical imaging technique characterized by the conversion of absorbed light to heat and then ultrasound waves via the photoacoustic effect. Following irradiation of an optical absorber, the excited state can relax via emission of a photon at a longer wavelength (fluorescence) or via non-radiative decay (photoacoustic). By pulsing the light source, pressure waves caused by thermoelastic expansion and contraction can be detected by ultrasound transducers and converted to high-resolution images. Since sound can readily propagate through tissue with minimal perturbation. PA tomography enables whole-body imaging of animals (e.g., mice), as well as human tissue (e.g., breast).2 In addition to a low fluorescent quantum yield (< 5%) and a large extinction coefficient (> 104 M-1cm-1), the intensity of the PA output relies on incident light reaching the optical absorber. While any wavelength of light can induce the generation of

a PA signal, absorbance above 650 nm is optimal for biological applications since the attenuation and scattering of incident light is minimal. For instance, in an optical imaging study, it was demonstrated that visible light at 510 nm can penetrate 1.5 mm into tissue, whereas light in the far-red (650 nm) and near infrared (>800 nm) regions can reach depths of 3 mm and 5-10 mm, respectively.³ Consequently, NIR dyes that absorb over 800 nm are desirable for deep tissue imaging.

Several NIR organic dyes have been explored for PA imaging, such as BODIPYs,⁴⁻⁷ squaraine,⁸⁻⁹ phthalocyanine and porphyrine,¹⁰⁻¹³ cyanines,¹⁴⁻¹⁵ benzo[c]heterocycles,¹⁶⁻¹⁷ and xanthene derivatives. 18-21 Amongst these, xanthenebased dyes are popular because of the tunability of their remarkable photophysical properties using organic synthesis. However, xanthene-based PA probes are scarce, especially those in the NIR region with absorbance >800 nm. Some examples include the seminaphthorhodafluor-5F PA probe with absorbance at 560 nm developed by Ashkenazi and coworkers for ratiometric pH sensing²² and the seminaphthorhodafluor-5F probe with absorption at 600 nm used by Wang and coworkers for quantitative imaging of tumor pH.18 Urano and coworkers developed a NIR Si-rhodamine PA probe with absorption at 780 nm for detecting hypochlorous acid,21 and some rhodol probes for PA imaging of quinone oxidoreductase activity at 700 nm were developed by Jiang and coworkers.²⁰ A rhodol nanoprobe with absorbance at 830 nm used for the ratiometric determination of Cu2+ was reported by Chen and coworkers.19 To our knowledge, this probe is the only reported xanthene-based PA probe with an absorption wavelength over 800 nm. While these dyes achieved their intentions, they either have short absorption wavelengths, relatively high fluorescent quantum yields, and/or arduous synthetic routes. With the limited quantities of xanthene-based PA probes available with absorbance over 800 nm and with the challenges that exist to prepare them in a facile and efficient way, there is a need for easily accessible NIR xanthene-based probes that can access imaging depths on the cm scale, possess low quantum yields, and are highly photostable for PA applications.

Herein, we report a new NIR xanthene-based PA imaging agent (XanthCR-880) with absorption maximum at 880 nm that extends into the NIR-II region. The dye was used in PA studies, where it exhibited excellent photostability and a readily detectable PA signal at depths up to 4 cm in a tissue overlay application.

Scheme 1. Synthesis of the XanthCR-880

We developed XanthCR-880 using the D-A-D design. The design of the dye was based on two factors: (i) a good overlap of the thiophene donor and xanthene acceptor to lower the bandgap of the dye due to charge transfer events,23-24 and (ii) an amino group connected to the thiophene to increase donor strength in the push-pull mechanism known to xanthene-based dyes. The dye was prepared from inexpensive commercially available materials in three simple steps that did not require tedious purification methods. The synthesis (Scheme 1) began with the coupling of 2-bromothiophene and piperidine using a copper catalyst to give compound 1 in 71% yield.25 Compound 1 was subjected to the direct C-H arylation reaction with 3',6'-dibromofluoran (2)26 to give compound 3 in 63 % yield. Treatment of compound 3 with TFA resulted in the opened form; however, to maintain the ring-opened form, compound 3 was esterified with ethanol according to our previously reported method²⁷ with slight modifications to give **XanthCR**-880 in 62 % yield. The dye and its precursors were characterized by ¹H NMR spectroscopy (Figure SI-1). The closed and opened forms of the dye can be differentiated by the shift in the resonance for the proton ortho to the carbonyl group on the spirolactone moiety; this proton's peak shifts downfield (~8.32 ppm) in the opened form compared to the closed form (~8.03 ppm). Additionally, the chemical shift of the C-9 carbon is different between the open and closed forms.

The absorption spectra of the closed and opened forms of the dye were obtained in dichloromethane (DCM) and dimethyl sulfoxide (DMSO) (**Figure 1**). The maximum

absorption wavelength (λ_{abs}) of the closed form (3) is 372 nm. However, when the dye was trapped in the opened form as the ethyl ester (XanthCR-880), the λ_{abs} shifted to 880 nm in DCM and 890 nm in DMSO, both of which are at the edge of the NIR I region and trail into the NIR II region. This is a significant bathochromic shift (508 nm) in DCM compared to the closed version. It should be noted that xanthene dyes having thienyl (4^+) and thieno[3,2-b]thienyl (5^+) rings as auxochrome were previously reported and exhibited absorption maxima ranging from 550 to 620 nm.28 Consequently, our design strategy with the thienylpiperidine donor resulted in a 300 nm red-shift in the absorption spectrum compared to the previously reported dye with just the thienyl donor. XanthCR-880 possesses high molar absorptivity of 88900 M⁻¹cm⁻¹ with a weak emission peak (λ_{em} 960 nm DMSO) in the NIR II region (Figure SI-2). Attempts to determine the fluorescent quantum yield were unsuccessful because of the exceedingly weak emission. Since a high extinction coefficient and a low quantum yield favor sound generation, we anticipated that XanthCR-880 would exhibit excellent PA properties.

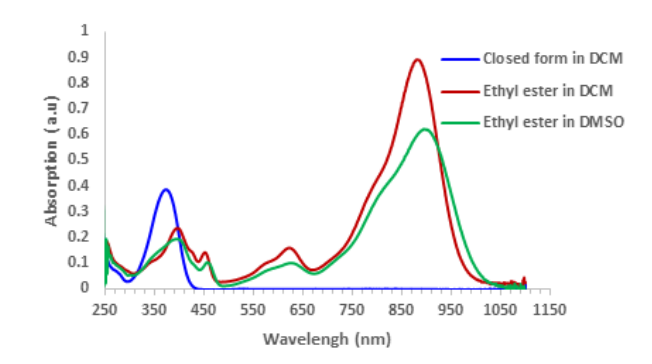


Figure 1. UV absorption spectra of 10 μM solution for the closed-form (3) and ethyl ester **XanthCR-880** version of the dye.

To probe the reason behind such a large difference in the absorption wavelength between **XanthCR-880** and **4**⁺, we performed time-dependent density functional theory (TDDFT) calculations on the acid analogues (Figure 2) of the two dyes using the ωB97X-D functional²⁹ and the def2-SVPD basis set (Figure SI-3 and 4).30 The calculations were performed using Q-Chem 5.3. The detachment and attachment densities for the lowest excitations in each molecule are shown in Figure 2, where the images were produced with VMD.³¹ The detachment density is the region that loses electron density during the excitation, and the attachment density is the region that gains electron density. Both molecules show a density shift from the thiophene rings toward the central region of the xanthene, which is attributed to π to π^* transitions. However, **XanthCR-880** also shows a net donation of electron density from the amine nitrogen atoms to the xanthene ring resulting in an increased effective conjugation length and increased charge transfer character of the transition. Both effects contribute to the large bathochromic shift in the absorption of XanthCR-880. The calculated electronic spectra of the dyes also show this red shift (Figure SI-5 and 6, respectively). XanthCR-880 was calculated to have an excitation energy of 2.18 eV, as compared

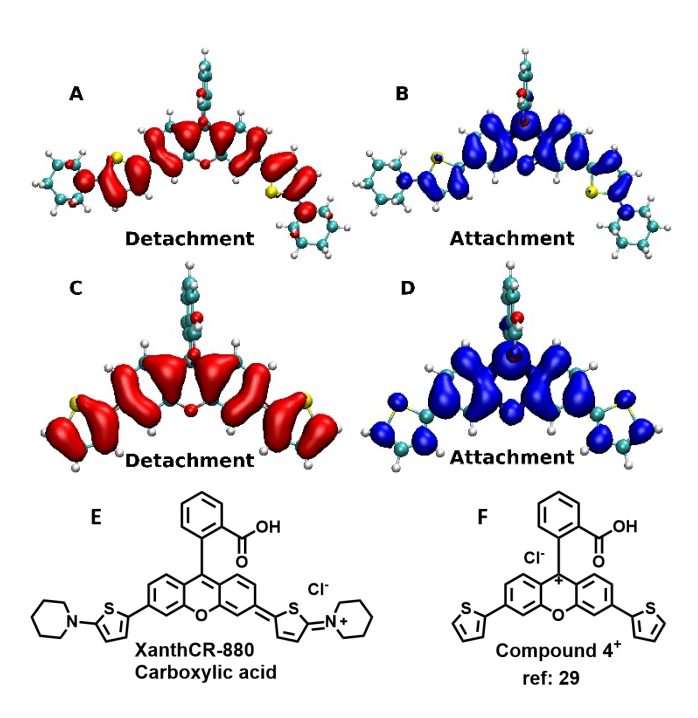


Figure 3. Detachment (A) and Attachment (B) densities for the acid analogue of the thienylpiperidine xanthene dye (**XanthCR-880 carboxylic acid**); Detachment (C) and Attachment (D) densities for the thienyl xanthene dye (**4**+). Structures of **XanthCR-880 carboxylic acid** (E) **and 4**+ (F)

to excitation energy of **4**+ (2.79 eV). This 0.61 eV red shift compares favourably with the experimental shift of 0.7 eV.

We tested the stability of our dye against glutathione, which is a potential reducing agent in biological media. We prepared the dye (17 μM) in 40% DMSO/60% PBS solution with 10 mM reduced glutathione and evaluated the change in the maximum absorption at 880 nm. The 10 mM concentration of reduced glutathione was selected to reflect the highest reported levels found in the body (i.e., liver).32 We observed no change in the absorbance of the dye after 30 min (Figure 3A); however, when the sample was further analyzed via LC-MS, a small quantity (< 10%) of the transesterified product (XanthCR-880, closed form) was observed. The presence of the closed form is attributed to an extended incubation time of 360 mins while waiting to acquire the data (Figure SI-7). These results suggest that the dye is stable to glutathione under the conditions and may be resistant to metabolic degradation by thiols in areas where glutathione levels are the highest. Furthermore, we evaluated the stability of XanthCR-880 in the presence of esterases, which can potentially hydrolyze the ethyl ester, resulting in the closed PA-inactive form. When XanthCR-880 was incubated at room temperature for 30 min with porcine liver esterase, no significant change in the absorbance was noted (Figure 3B). We also evaluated the dye for its compatibility as a PA contrast agent in chloroform (Figure 3C) and PBS buffer (Figure SI-8) and observed that the strongest intensity (λ_{PA}) was at 890 and 865 nm, respectively. It is common for the λ_{PA} value to differ slightly from the corresponding λ_{abs} based on empirical observation. Since the appearance of both PA spectra feature sharp peaks characteristic of xanthene-based dyes, we postulate that XanthCR-880 exists predominantly in a non-aggregated state under

these conditions. This is an important consideration because aggregates are associated with weaker PA signals owing to significant broadening of the absorbance band and a corresponding decrease of the molar absorptivity. In the presence of PBS solution without SDS, we observed the formation of blue-shifted H-aggregates with a λ_{abs} centered at 740 nm. However, inclusion of an organic cosolvent (DMF), which was varied from 0% to 30%, recovered the non-aggregated state (Figure SI-9). Next, we established that there was a linear relationship between dye concentration and the PA signal up to the highest concentration tested (2.0 μ M) and a limit of detection of 0.36 μ M in ethanol (Figure **3D**). These results are comparable to what was previously reported using indocyanine green (ICG).33 Unlike ICG, XanthCR-880 does not feature water solubilizing sulfonate groups, demonstrating its intrinsic solubility. For any PA contrast agent to find utility in studies where it may be subjected to multiple imaging sessions, it must be resistant to photobleaching. When XanthCR-880 was continuously irradiated at its λ_{PA} for 60 mins, we found that the PA signal decreased by only 45 %, indicating that XanthCR-880 is exceptionally photostable (Figure 3E).

Spectral unmixing is a technique employed to isolate the signal of a PA contrast agent from that of other PA-active molecules such as hemoglobin found in blood. For these measurements, a well-defined PA spectrum is required.

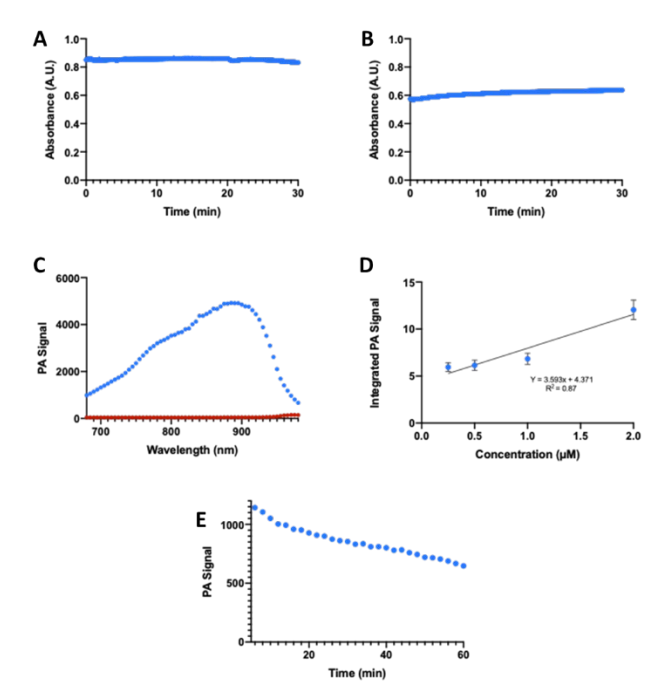


Figure 2. Absorption studies showing the stability of **XanthCR880** (20 μM) to treatment of glutathione (10 mM) (A) and esterase (5 units) (B). Both experiments were conducted at room temperature for 30 mins. Photoacoustic spectrum of **XanthCR-880** (20 μM) in CHCl₃ (blue) and a vehicle control (red), λ_{PA} = 890 nm (C). Integrated photoacoustic signal of **XanthCR-880** at 0.25, 0.5, 1.0 and 2.0 μM in EtOH (D). The LOD was determined to be 0.36 μM according to the following equation (LOD = 3 × blank × SD of slope/(1-slope)². Photobleaching of **XanthCR-880** (20 μM) in CHCl₃ under continuous irradiation at 880 nm (E).

Along these lines, a λ_{abs} above 800 nm presents an opportunity to simultaneously detect two biomarkers via multiplex imaging using two different dyes. To evaluate this possibility, we added XanthCR-880 into one tube and an aza-BODIPY reference dye (λ_{PA} = 680 nm) (**Figure 4A**) to another. Each dye could be induced to generate a PA signal when both samples were irradiated at a common excitation wavelength (690 nm) (Figure 4B). In this instance, the signal from the aza-BODIPY is stronger than XanthCR-880 because the excitation wavelength was set at the λ_{PA} of the reference. As shown in **Figure 4B** it would not be possible to distinguish XanthCR-880 from the other dye without prior knowledge of their identity or concentration. However, by employing the PA spectrum described above (in DCM), we were able to readily separate the signal of XanthCR-880 from the aza-BODIPY via spectral unmixing (Figure 4C).

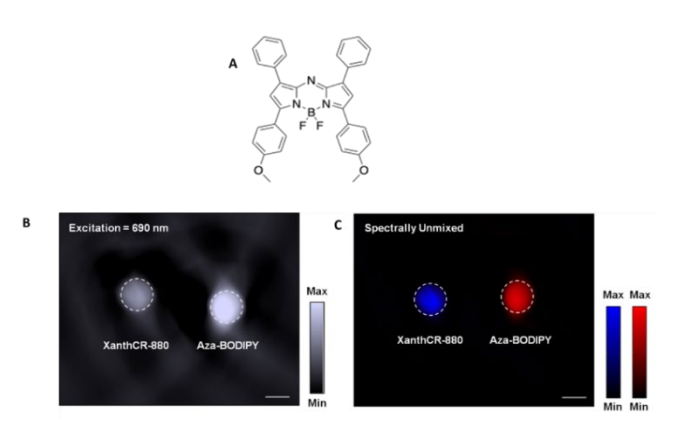


Figure 4. Standard dimethoxy aza-BODIPY dye (λ_{abs} = 688 nm, ϵ = 78,300 M⁻¹ cm⁻¹ measured in CHCl₃ (A). Representative photoacoustic image of **XanthCR-880** (20 μ M) and aza-BODIPY dye (20 μ M) overlayed with a 1 cm thick agar tissue phantom (10% milk by volume) and irradiated at 690 nm (B). Image processed via multispectral unmixing where the signal from **XanthCR-880** is shown in blue and the signal from the aza-BODIPY dye is colored in red (C). All images were acquired using a MSOT inVision 128 system (iThera Medical). Scale bar represents 2 mm.

Typically, when newly developed dyes are tested for their PA properties, we overlay them with a tissue mimicking phantom casted from agar containing 10% milk by volume. While this setup is efficient at scattering the incident light to provide even illumination of a sample, it lacks strong optical absorbers found in tissue that can attenuate light. As such, we designed a better challenge to test the maximum attainable imaging depth. Specifically, XanthCR-880 was overlayed with swine tissue of varying thickness (1 to 4 cm). We hypothesized that we could image XanthCR-880 beyond a depth of 1 cm owing to its strong PA intensity in the NIR region. Indeed, we were able to detect a robust signal even at tissue thickness of 4 cm (Figure 5). This significant result demonstrates that XanthCR-880 possesses a substantially strong PA signal necessary for deep tissue PA imaging.

We developed a new xanthene-based dye using the D-A-D strategy with a thienylpiperidine unit, which is a strong donor, and the xanthene core as the acceptor. We achieved λ_{abs} and λ_{em} in the NIR I region and established that the dye is highly photostable. In agreement with the experimental

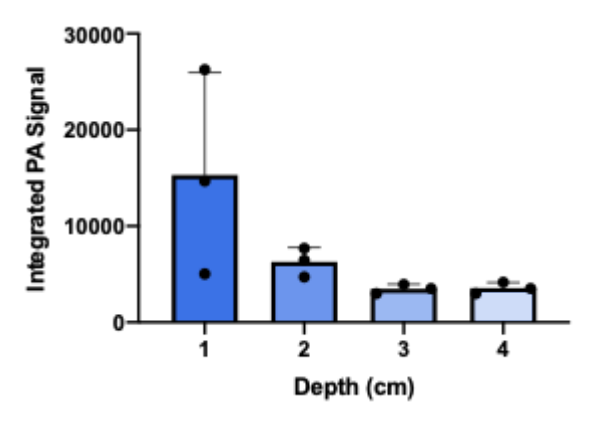


Figure 5. Integrated photoacoustic signal of **XanthCR-880** (20 μ M) in PBS with 0.1% SDS overlayed with swine tissue with a thickness of 1, 2, 3, or 4 cm. Error = standard deviation. For experiments in a-c, **XanthCR-880** was placed in fluorinated ethylene propylene (FEP) tubing, overlayed with 1 cm thick agar-based tissue phantom and imaged at 25 °C.

data, TDDFT calculations of the excitation spectra revealed a large bathochromic shift of our **XanthCR-880** dye compared to the reported **4**+ dye. Furthermore, the dye is resistant to high concentration of glutathione and esterases, suggesting that it would be stable in biological environment. **XanthCR-880** gave a weak emission signal; however, the PA signal was very intense and the λ_{PA} is in the NIR region in organic and aqueous media. **XanthCR-880** is compatible with multiple PA imaging systems and produced good PA signals even at depth of 4 cm in tissue. This is the longest wavelength xanthene-based PA dye to date.

ASSOCIATED CONTENT

Supporting Information

The Supporting Information is available free of charge on the ACS Publications website.at https://pubs.acs.org.

¹H NMR, ¹³C NMR (PDF), UV/Vis (PDF), Cartesian coordinates and singlet excited states, PA studies (PDF), and MTT studies (PDF)

AUTHOR INFORMATION

Corresponding Author

* Colleen N. Scott - Department of Chemistry, Mississippi State University, Mississippi State, MS 39762, United States. Email: cscott@chemistry.msstate.edu

* Jefferson Chan - Department of Chemistry, University of Illinois at Urbana-Champaign, Urbana, IL 61801, United States. Email: jeffchan@illinois.edu

Author Contributions

Chathuranga S. L. Rathnamalala‡, Bailey S. Herring, Mattea Hooper, and Steven R. Gwaltney - Department of Chemistry, Mississippi State University, Mississippi State, MS 39762,, United States

Nicholas W. Pino‡ - Department of Chemistry, University of Illinois at Urbana–Champaign, Urbana, IL 61801, United States ‡These authors contributed equally

The authors declare no competing financial interest.

ACKNOWLEDGMENT

Funding Sources: The authors are grateful to the National Science Foundation for award OIA-1757220 that funded this research. J.C. acknowledges the National Institutes of Health for support (R35GM133581). N.W.P. thanks the Chemistry-Biology Interface Training Grant (T32-GM136629), Robert C. and Carolyn J. Springborn Graduate Fellowship, and the Tissue Microenvironment Training Grant (T32 EB019944) for support.

REFERENCES

- 1. Wang, L. V.; Hu, S., Photoacoustic Tomography: In Vivo Imaging from Organelles to Organs. *Science* **2012**, *335* (6075), 1458.
- 2. Attia, A. B. E.; Balasundaram, G.; Moothanchery, M.; Dinish, U. S.; Bi, R.; Ntziachristos, V.; Olivo, M., A review of clinical photoacoustic imaging: Current and future trends. *Photoacoustics* **2019**, *16*, 100144.
- 3. Teraphongphom, N.; Kong, C. S.; Warram, J. M.; Rosenthal, E. L., Specimen mapping in head and neck cancer using fluorescence imaging. *Laryngoscope Investig Otolaryngol* **2017**, *2* (6), 447-452.
- 4. Merkes, J. M.; Lammers, T.; Kancherla, R.; Rueping, M.; Kiessling, F.; Banala, S., Tuning Optical Properties of BODIPY Dyes by Pyrrole Conjugation for Photoacoustic Imaging. *Advanced Optical Materials* **2020**, *8* (11), 1902115.
- 5. Shi, B.; Gu, X.; Fei, Q.; Zhao, C., Photoacoustic probes for real-time tracking of endogenous H2S in living mice. *Chemical Science* **2017**, *8* (3), 2150-2155.
- 6. Ou, C.; Zhang, Y.; Ge, W.; Zhong, L.; Huang, Y.; Si, W.; Wang, W.; Zhao, Y.; Dong, X., A three-dimensional BODIPY-iron(iii) compound with improved H2O2-response for NIR-II photoacoustic imaging guided chemodynamic/photothermal therapy. *Chemical Communications* **2020**, *56* (46), 6281-6284.
- 7. Zhou, E. Y.; Knox, H. J.; Liu, C.; Zhao, W.; Chan, J., A Conformationally Restricted Aza-BODIPY Platform for Stimulus-Responsive Probes with Enhanced Photoacoustic Properties. *Journal of the American Chemical Society* **2019**, *141* (44), 17601-17609.
- 8. An, F.-F.; Deng, Z.-J.; Ye, J.; Zhang, J.-F.; Yang, Y.-L.; Li, C.-H.; Zheng, C.-J.; Zhang, X.-H., Aggregation-Induced Near-Infrared Absorption of Squaraine Dye in an Albumin Nanocomplex for Photoacoustic Tomography in Vivo. *ACS Applied Materials & Interfaces* **2014**, *6* (20), 17985-17992.
- 9. Yao, D.; Wang, Y.; Zou, R.; Bian, K.; Liu, P.; Shen, S.; Yang, W.; Zhang, B.; Wang, D., Molecular Engineered Squaraine Nanoprobe for NIR-II/Photoacoustic Imaging and Photothermal Therapy of Metastatic Breast Cancer. *ACS Applied Materials & Interfaces* **2020**, *12* (4), 4276-4284.
- 10. Lovell, J. F.; Jin, C. S.; Huynh, E.; Jin, H.; Kim, C.; Rubinstein, J. L.; Chan, W. C. W.; Cao, W.; Wang, L. V.; Zheng, G., Porphysome nanovesicles generated by porphyrin bilayers for use as multimodal biophotonic contrast agents. *Nature Materials* **2011**, *10* (4), 324-332.
- 11. Shimomura, K.; Kai, H.; Nakamura, Y.; Hong, Y.; Mori, S.; Miki, K.; Ohe, K.; Notsuka, Y.; Yamaoka, Y.; Ishida, M.; Kim, D.; Furuta, H., Bis-Metal Complexes of Doubly N-Confused Dioxohexaphyrins as Potential Near-Infrared-II Photoacoustic Dyes. *Journal of the American Chemical Society* **2020**, *142* (9), 4429-4437.
- 12. Zheng, X.; Wang, L.; Liu, S.; Zhang, W.; Liu, F.; Xie, Z., Nanoparticles of Chlorin Dimer with Enhanced Absorbance for Photoacoustic Imaging and Phototherapy. *Advanced Functional Materials* **2018**, *28* (26), 1706507.
- 13. Merkes, J. M.; Rueping, M.; Kiessling, F.; Banala, S., Photoacoustic Detection of Superoxide Using Oxoporphyrinogen and Porphyrin. *ACS Sensors* **2019**, *4* (8), 2001-2008.
- 14. Li, X.; Tang, Y.; Li, J.; Hu, X.; Yin, C.; Yang, Z.; Wang, Q.; Wu, Z.; Lu, X.; Wang, W.; Huang, W.; Fan, Q., A small-molecule probe for ratiometric photoacoustic imaging of hydrogen sulfide in living mice. *Chemical Communications* **2019**, *55* (42), 5934-5937.
- 15. Gao, W.; Li, X.; Liu, Z.; Fu, W.; Sun, Y.; Cao, W.; Tong, L.; Tang, B., A Redox-Responsive Self-Assembled Nanoprobe for Photoacoustic

- Inflammation Imaging to Assess Atherosclerotic Plaque Vulnerability. *Analytical Chemistry* **2019**, *91* (1), 1150-1156.
- 16. Lu, Y.; Sun, Q.; Zhang, Z.; Tang, L.; Shen, X.; Xue, S.; Yang, W., New frog-type Dibenzo[a,c][1,2,5]thiadiazolo[3,4-i]phenazine heterocyclic derivatives with aggregation-enhanced one- and two-photon excitation NIR fluorescence. *Dyes and Pigments* **2018**, *153*, 233-240.
- 17. Zhang, R.; Wang, Z.; Xu, L.; Xu, Y.; Lin, Y.; Zhang, Y.; Sun, Y.; Yang, G., Rational Design of a Multifunctional Molecular Dye with Single Dose and Laser for Efficiency NIR-II Fluorescence/Photoacoustic Imaging Guided Photothermal Therapy. *Analytical Chemistry* **2019**, *91* (19), 12476-12483.
- 18. Jo, J.; Lee, C. H.; Kopelman, R.; Wang, X., In vivo quantitative imaging of tumor pH by nanosonophore assisted multispectral photoacoustic imaging. *Nature Communications* **2017**, *8* (1), 471.
- 19. Wang, S.; Yu, G.; Ma, Y.; Yang, Z.; Liu, Y.; Wang, J.; Chen, X., Ratiometric Photoacoustic Nanoprobe for Bioimaging of Cu2+. *ACS Applied Materials & Interfaces* **2019**, *11* (2), 1917-1923.
- 20. Liu, F.; Shi, X.; Liu, X.; Wang, F.; Yi, H.-B.; Jiang, J.-H., Engineering an NIR rhodol derivative with spirocyclic ring-opening activation for high-contrast photoacoustic imaging. *Chemical Science* **2019**, *10* (40), 9257-9264
- 21. Ikeno, T.; Hanaoka, K.; Iwaki, S.; Myochin, T.; Murayama, Y.; Ohde, H.; Komatsu, T.; Ueno, T.; Nagano, T.; Urano, Y., Design and Synthesis of an Activatable Photoacoustic Probe for Hypochlorous Acid. *Analytical Chemistry* **2019**, *91* (14), 9086-9092.
- 22. Horvath, T. D.; Kim, G.; Kopelman, R.; Ashkenazi, S., Ratiometric photoacoustic sensing of pH using a "sonophore". *Analyst* **2008**, *133* (6), 747-749.
- 23. Kinnibrugh, T. L.; Salman, S.; Getmanenko, Y. A.; Coropceanu, V.; Porter, W. W.; Timofeeva, T. V.; Matzger, A. J.; Brédas, J.-L.; Marder, S. R.; Barlow, S., Dipolar Second-Order Nonlinear Optical Chromophores Containing Ferrocene, Octamethylferrocene, and Ruthenocene Donors and Strong π -Acceptors: Crystal Structures and Comparison of π -Donor Strengths. *Organometallics* **2009**, *28* (5), 1350-1357.
- 24. Qian, G.; Wang, Z. Y., Near-Infrared Organic Compounds and Emerging Applications. *Chemistry An Asian Journal* **2010**, *5* (5), 1006-1029.
- 25. Lu, Z.; Twieg, R. J., A mild and practical copper catalyzed amination of halothiophenes. *Tetrahedron* **2005**, *61* (4), 903-918.
- 26. Roger, J.; Doucet, H., Aryl triflates: useful coupling partners for the direct arylation of heteroaryl derivatives via Pd-catalyzed C-H activation-functionalization. *Organic & Biomolecular Chemistry* **2008**, *6* (1), 169-174.
- 27. Rathnamalala, C. S. L.; Gayton, J. N.; Dorris, A. L.; Autry, S. A.; Meador, W.; Hammer, N. I.; Delcamp, J. H.; Scott, C. N., Donor-Acceptor-Donor NIR II Emissive Rhodindolizine Dye Synthesized by C-H Bond Functionalization. *The Journal of Organic Chemistry* **2019**, *84* (20), 13186-13193.
- 28. Matsui, M.; Yamamoto, T.; Kakitani, K.; Biradar, S.; Kubota, Y.; Funabiki, K., UV-vis absorption and fluorescence spectra, solvatochromism, and application to pH sensors of novel xanthene dyes having thienyl and thieno[3,2-b]thienyl rings as auxochrome. *Dyes and Pigments* **2017**, *139*, 533-540.
- 29. Chai, J.-D.; Head-Gordon, M., Long-range corrected hybrid density functionals with damped atom-atom dispersion corrections. *Physical Chemistry Chemical Physics* **2008**, *10* (44), 6615-6620.
- 30. Rappoport, D.; Furche, F., Property-optimized Gaussian basis sets for molecular response calculations. *The Journal of Chemical Physics* **2010**, *133* (13), 134105.
- 31. Humphrey, W.; Dalke, A.; Schulten, K., VMD: visual molecular dynamics. *J Mol Graph* **1996**, *14* (1), 33-8, 27-8.
- 32. Forman, H. J.; Zhang, H.; Rinna, A., Glutathione: overview of its protective roles, measurement, and biosynthesis. *Mol Aspects Med* **2009**, *30* (1-2), 1-12.
- 33. Kanazaki, K.; Sano, K.; Makino, A.; Takahashi, A.; Deguchi, J.; Ohashi, M.; Temma, T.; Ono, M.; Saji, H., Development of human serum albumin conjugated with near-infrared dye for photoacoustic tumor imaging. *Journal of Biomedical Optics* **2014**, *19* (9), 096002.